

Design of a portable near infrared system for topographic imaging of the brain in babies

Tharshan Vaithianathan,^{a)} Iain D. C. Tullis, Nicholas Everdell, Terence Leung, and Adam Gibson

Department of Medical Physics and Bioengineering, University College London, London WC1E 6JA, United Kingdom

Judith Meek

Department of Paediatrics and Child Health, University College London, 5 University Street, London WC1E 6JJ, United Kingdom

David T. Delpy

Department of Medical Physics and Bioengineering, University College London, London WC1E 6JA, United Kingdom

(Received 9 June 2003; accepted 13 May 2004; published 22 September 2004)

A portable topographic near-infrared spectroscopic (NIRS) imaging system has been developed to provide real-time temporal and spatial information about the cortical response to stimulation in unrestrained infants. The optical sensing array is lightweight, flexible, and easy to apply to infants ranging from premature babies in intensive care to children in a normal environment. The sensor pad consists of a flexible double-sided circuit board onto which are mounted multiple sources (light-emitting diodes) and multiple detectors (*p-i-n* photodiodes), all electrically encapsulated in silicone rubber. The control electronics are housed in a box with a medical grade isolated power supply and linked to a PC fitted with a data acquisition card, the signal acquisition and analysis being performed using LABVIEW™. The signal output is displayed as an image of oxy- and deoxyhemoglobin concentration ($[\text{HbO}_2]$, $[\text{Hb}]$) changes at a frame rate of 3 Hz. Experiments have been conducted on phantoms to determine the sensitivity of the system, and the results have been compared to theoretical simulations. The system has been tested in volunteers by imaging changes in forearm muscle oxygenation, following blood pressure cuff occlusion to obtain typical $[\text{Hb}]$ and $[\text{HbO}_2]$ plots. © 2004 American Institute of Physics. [DOI: 10.1063/1.1775314]

I. INTRODUCTION

Techniques such as electroencephalography (EEG), positron emission tomography (PET), functional magnetic resonance imaging (fMRI), or magnetoencephalography (MEG) can be used to noninvasively investigate cerebral function. Although these techniques are widely used clinically, the instruments are very expensive, require specially trained technical staff to operate, and with the exception of EEG, patients have to be moved from their ward and taken to specially constructed rooms where the investigation is carried out. In the case of PET, patients have to be injected with radioisotopes, which prevent multiple repeated studies. All of these factors make these imaging modalities unsuitable and inconvenient for imaging cerebral functions in babies in real time, especially if they are being cared for in an intensive care unit.

Near-infrared spectroscopy (NIRS) is an optical method of noninvasively measuring cerebral function at the bedside. It is a useful technique to investigate biological tissues, because in the near-infrared region (750–900 nm), water has a low absorption, while oxyhemoglobin (Hb) and deoxyhemoglobin (HbO_2) still have detectable absorption differences.

As a result, near-infrared light can penetrate several centimeters of biological tissues, enabling noninvasive investigation of the brain from the surface of the scalp. It is a relatively simple technique that is portable, does not require a dedicated technical staff, and does not require the patient to be injected with any isotopes.

Several different types of NIR instruments have been developed over the past 20 years to measure changes in cerebral oxygenation, perfusion, and more recently, to image brain activity.^{1–5} These instruments, whether they just monitor nonlocalized signal changes, or produce topographic two-dimensional (2D) or tomographic three-dimensional (3D) images of activity in the brain, can generally be classified into three major categories: time-resolved,^{6–13} frequency modulated,^{14–22} and continuous intensity^{23–27} instruments. Time-resolved instruments involve injecting short pulses of light (typically a few picosecond duration) and measuring the distribution of flight times of the transmitted photons, a parameter known as the temporal point spread function. This measurement provides the greatest amount of information about the tissue being interrogated, although the instrumentation needed is both complex and expensive. Frequency modulated instruments involve modulating the light source at radio frequencies and detecting the intensity and phase of the transmitted signal. This requires less complex and expensive

^{a)}Electronic mail: tharshan@unisa.edu.au

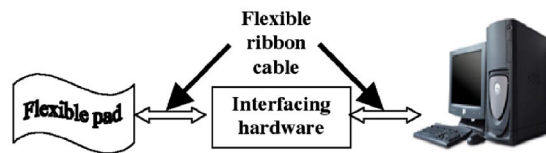


FIG. 1. (Color online) Overall system.

instrumentation. The third and simplest type of measurement system is the continuous intensity instrument, where light is injected into the tissue and the attenuated transmitted intensity is measured at some distance from the source.

The aim of the work described in this paper was to develop a simple intensity based NIR instrument that could be used on preterm and term babies to produce a 2D topographic image of the cortical response to stimulation. We have previously shown using a single-channel continuous intensity measurement instrument, Hamamatsu NIRO 300, that visually evoked responses can be obtained in the occipital cortex in babies.³ This instrument uses a single light source with a single detector and measures the hemodynamic changes occurring in the region between the source and detector. The limitation of this instrument is that precise placement of the source and detector is required in order to monitor the correct hemodynamic changes in an evoked response study. Hence, although different parts of the brain could respond to a stimulus, the instrument may not detect the resulting changes if the source and detector are not placed accurately over the activated region. In the infant, where the brain is still developing and the head shape is still changing, it is difficult to predict where the cerebral activation may occur, and in serial studies this may also change with time as cortical development continues. However, by using an array system with multiple sources and multiple detectors, regional changes can be monitored, enabling the precise location of activation regions of the brain. Because of the need to study the infants in a wide variety of situations, ranging from the neonatal intensive care unit to a near home environment, it was also essential that the measurement instrument be portable, lightweight, easy to use, and ideally inexpensive.

II. INSTRUMENT DESCRIPTION

The overall system design is shown in Fig. 1. The sensor array consists of multiple sources and multiple detectors placed on a flexible circuit board (flexible pad) that conforms easily to the shape or size of a baby's head. The flexible pad has dimensions of 8×4 cm, which covers the entire region of the visual cortex of both preterm and term babies. A long (1-m) flexible ribbon cable connects the pad to the interfacing hardware, enabling the baby to move if required.

Light sources at two different wavelengths are required in order to resolve both oxyhemoglobin (HbO_2) and the deoxyhemoglobin (Hb) changes. The maximum intensity of light that can be safely delivered to a biological tissue is limited to a few milliwatts, however the *peak* intensity of light delivered to the tissue can exceed this by several orders of magnitude if the sources are pulsed. To speed up data acquisition, the attenuated signal can also be measured simultaneously on more than one detector. This is easily

achieved using a sample and hold circuit, where, as each source is pulsed, the signals from all of the detectors are "held." By pulsing a number of sources simultaneously, the overall data acquisition time can be further reduced, provided the distance between the sources that are on simultaneously is sufficiently large that there is negligible risk of cross talk (i.e., a detector picking up a signal from more than one source). The detected signals are amplified using transimpedance amplifiers and transferred to a PC via a data acquisition card with appropriate software and interfacing electronics.

III. FLEXIBLE PAD

As mentioned, all the light sources and detectors are mounted on a flexible pad measuring 8×4 cm.

A. Light sources

Three types of light sources were considered: laser diodes, white light sources with filters, or light-emitting diodes (LEDs). *Laser diodes* have been used in NIRS for imaging system by several groups.^{11,23,28,29} However, they are both relatively expensive and require optical fiber coupling to the sensor array, which can be difficult when it comes to attaching onto a baby's head,^{28,30} as custom designed caps or holders may be necessary and the fibers can be fragile and easily broken. *White light sources* require appropriate filters, and are also bulky and hence difficult to fit within the small space available. They also pose significant heat dissipation problems. *LEDs*, on the other hand, can be obtained in small packages and several of them can be easily fitted into a small region with minimal heat dissipation problems.²²

The specification required of the LEDs is that they be of high power and have a narrow spectral bandwidth. It has been shown previously that the optimum pair of wavelengths to use are 664 and 830 nm.³¹ No suitable LEDs were available at exactly these wavelengths, but LEDs of relatively narrow spectral bandwidth (40 nm) at 780 nm (OD-7860) and 880 nm (OD-8860) were available from Optodiode Corporation, which when pulsed (0.5 A for 10 μs at 200 Hz) produced a peak power output of 8 mW.

B. Detectors

Four types of detectors that can be used to measure the transmitted signals are available: silicon photodiodes, avalanche photodiodes (APDs), photomultiplier tubes (PMTs), and charge coupled devices (CCDs). The latter two options were not feasible on the basis of price and size. Although silicon photodiodes have a lower sensitivity in comparison to APDs, their reasonable response time, high dynamic range, and the requirement that several needed to be placed within the flexible pad area of 8×4 cm made them the optimum choice. In order to minimize the physical chip size, the active collecting area had to be as large as possible with negligible dead space. Silicon sensor (SSO-PDQ-20-6-ch) *p-i-n* photodiodes best satisfied these requirements, with a collection area of 20 mm², a dead space of only 0.3 mm², and a low dark current of typically 2 nA.

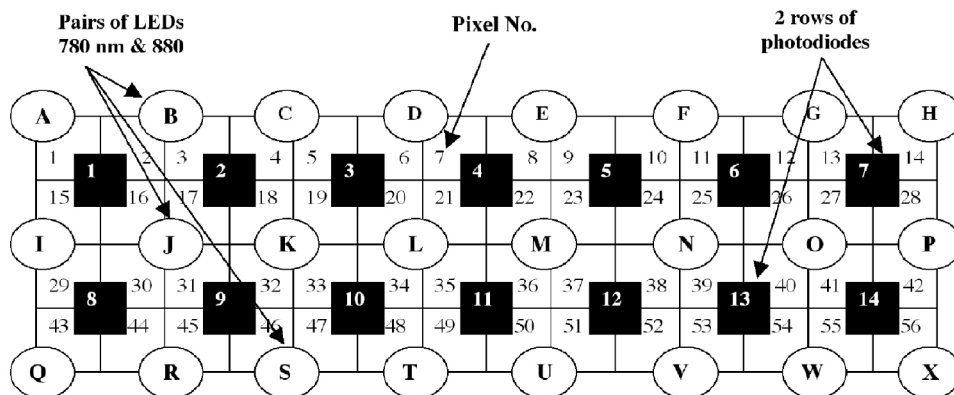


FIG. 2. (Color online) The arrangement of 24 pairs of LEDs (A–X) and 14 photodiodes on the flexible pad, including the pixel numbers (1–56) used for software display.

The sensor array finally consisted of 48 LEDs and 14 photodiodes mounted on a flexible circuit board with the LEDs arranged in three rows of 16 (eight pairs of LEDs, one at 780 nm and the other at 880 nm), and the photodiodes arranged in two rows of seven, with the distance between the pairs of LEDs being 1 cm (Fig. 2).

C. Amplifier

Photodiodes generate low level current that is proportional to the level of illumination, and these signals need to be amplified. A number of amplifier configurations are discussed in great detail by Graeme³² and after considering several options, it was decided that a single stage transimpedance amplifier was most suitable. This offers better linearity, greater bandwidth, and also produces lower offset voltages, in comparison to the voltage gain configuration. Low distortion amplifiers with FET inputs were considered, and their individual noise performances were calculated (based on a feedback resistor of 100 k Ω). The OPA2604 (Burr Brown), a dual FET input, low distortion amplifier, was the best choice in terms of noise performance, physical dimensions, and availability. The transimpedance amplifiers should be as close as possible to the photodiodes to minimize noise pickup, but because of the limited space on the sensor pad, and the requirement for maximum pad flexibility as outlined above, the amplifier could not be placed next to photodiode on the printed circuit board (pcb). However, the photodiode and amplifier have similar physical dimensions, and therefore the amplifiers could be placed on the other side of the pcb, directly behind the photodiodes. This has two advantages. First, it reduces stray capacitance, minimizes channel-to-channel cross talk, and reduces noise pickup from the surrounding circuitry. Second, the combination provides mechanical support for the photodiodes (in the form of a rigid hard backing), ensuring that they will not become detached when the circuit board is flexed. To further minimize the risk of detachment, an additional layer of cover lay was put on the back of the pcb behind the LEDs to act as a further mechanical support. The feedback resistors (100 k Ω) on the transimpedance amplifiers, together with gain compensating feedback capacitors of 6.5 pF, are also placed on the flexible pad. Since the LEDs are pulsed with a current pulse of 10- μ s width, hence the required 3-db gain was 1 MHz (i.e., the measured signal should settle within one-tenth of the time of the pulse width).

D. Flexible head pad

One of the design challenges in this project was to accommodate all of the electronic components (96) and signal lines (113) into the 8 \times 4 cm region, while at the same time retaining the flexibility of the pad to enable it to conform to the shape and size of an infant's head [Fig. 3(a)]. All 48 LEDs and 14 photodiodes (in the front of the pad) could not be placed vertically in columns or horizontally next to each other, as this was found to greatly reduce the flexibility of the pad. Placing the LEDs and photodiodes in a staggered arrangement increases the flexibility. The minimum spacing between the LEDs and photodiodes is determined by the number of tracks that can be placed between components.

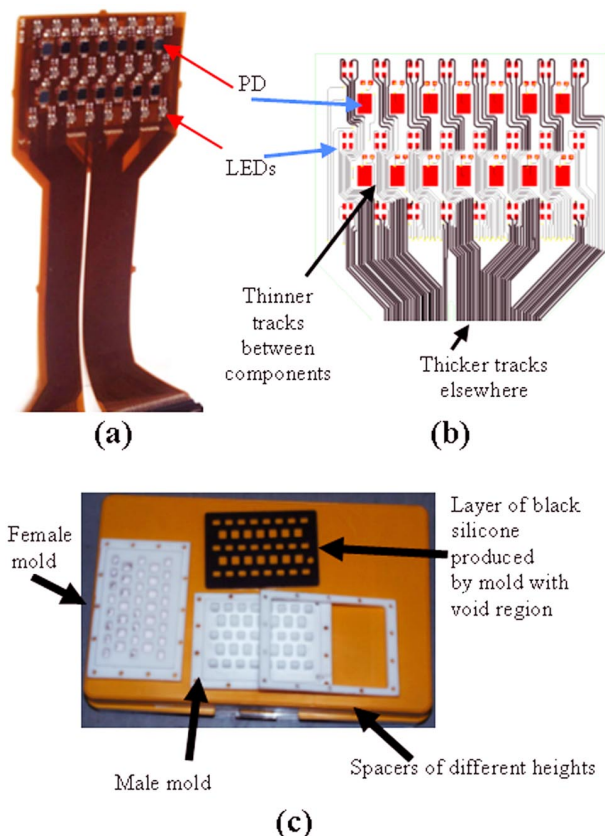


FIG. 3. (Color online) Flexible pad. (a) Front of flexible pad with all 48 LEDs and 14 photodiodes, (b) track layout where thinner tracks have been used between components and thicker tracks elsewhere, and (c) mold used for encapsulating front of flexible pad.

This was a significant challenge, since the track width in the LED connections cannot be made arbitrarily small, as a tradeoff exists between track width and voltage drop along the length of the track (a 30-cm-long, 0.127-cm-width track made with 17.5- μm -thick copper, will have a voltage drop of 1.14 V if 1 A is pulsed through it). Another means of fitting several tracks into a small area is to use a multilayered board, where tracks can be distributed among the different layers. However, as the number of layers increase, the thickness of the flexiboard increases (two-, four-, or six-layered boards have a thickness of 17.7, 38.2, and 52.6 μm , respectively), again compromising the flexibility of the pad. Therefore, the flexibility depends ultimately on the number of layers, the thickness of the copper tracks, the number of tracks, and also on the material used to manufacture the circuit board. In light of these factors, a two-layered board was chosen, with 35- μm -thick copper tracks (to cater for the high pulsed current), with short sectors of thinner track (0.254 cm) used in regions between components, and thicker tracks (0.508 cm) used elsewhere [Fig. 3(b)].

E. Encapsulation of head pad

The flexible circuit board cannot be placed in direct contact with the patient, as it contains electronic components. It requires encapsulation in a suitable material which should: (a) be flexible enough to conform to the baby's head (maximum of 35 Shore hardness), (b) have suitable optical properties, (c) have a low viscosity enabling it to be poured into a mold, (d) have a long working time and a short curing time, and (e) not give off any by-products during curing that will degrade the flexible pcb or the components (some encapsulants produce acetic acid as a by product).

A two-part clear silicon rubber (RTV615, GE Silicon) satisfied all of the above requirements. Black pigment (Alec Tiranti Ltd.) had to be added to the clear mixture to ensure that no lateral leakage of light could occur from source to detector, so that all of the light detected must have traveled through the tissue being interrogated.

Encapsulation had to be carried out in three stages: (a) encapsulation of the back of the pad with the transimpedance amplifiers, (b) encapsulating the front of the flexible board, except for the regions directly above the LEDs and photodiodes, and (c) filling the regions directly above the LEDs and photodiodes. RTV615 containing the black pigment was first poured over the rear of the pad, which was held in a custom made PTFE mold and left to cure overnight (mold not shown). A separate two-part PTFE mold [Fig. 3(c)] was designed to cast the rubber for the front of the pad. This mold has a male and female counterpart, and produces a layer of black silicon rubber, with an array of void regions. The void regions are areas where the LEDs and photodiodes are eventually situated. Varying thicknesses of the silicon rubber can be produced, using spacers of different heights, but a thickness of 2 mm was used in the pad described here. Once cured, this molding was attached to the front of the pad using a thin layer of the black RTV as an adhesive. Once this was cured, the void regions above the LEDs and photodiodes were filled with clear silicon rubber.

IV. INTERFACING HARDWARE

The interfacing hardware consists of three LED driver boards, one isolation board, and a switch mode power supply, all encompassed in a small ($29 \times 26 \times 17$ cm) plastic box (Meditec 220, OKW Enclosures Ltd.).

A. LED driver boards

Our design incorporates three LED driver boards, each controlling a single row of LEDs (a single row consists of eight pairs, where a single pair consists of LEDs at 780 and 880 nm). A digital output from the data acquisition board (PCI-DAS1602/16, Computerboards) card provides the trigger required for a monostable multivibrator to produce short 10- μs pulses. This pulse is fed into a demultiplexer that selects one of eight LEDs, and then into a FET, via a high-speed FET driver to turn each of the LEDs "on" and "off."

An octal 8-bit digital-to-analog converter (DAC) (MX7228TQ, Maxim) provides individual current drive for the LEDs, as it contains eight separate latches with output buffers that can be individually addressed using three digital outputs from the computer. Using four of the maximum eight bits, it is possible to set 16 different levels of current drive for the LEDs. Two DACs are required on each board: one to control the 780 nm and the other the 880-nm LEDs. The output of the DAC drives an adjustable voltage regulator (one per LED). A 10- μF capacitor on the output of each voltage regulator supplies the instantaneous peak current for the LEDs.

B. Isolation board

The complete measurement system has to conform to the European medical isolation standards (EN60601-1). To this end, the isolation board contains optoisolators, isolating all of the digital signals *from* the computer, and a single low distortion 120-kHz bandwidth isolation amplifier, which relays the photodiode signal back *into* the computer. The signals from all of the 14 photodiodes are fed into a sample and hold circuit, which enables all photodiodes to be either "sampled" or "held" simultaneously. The outputs of the sample and hold are fed via a 16-channel multiplexer to the computer after isolation. Finally, the layout of the components and tracks are such that there is a clear 8-mm gap between the isolated and nonisolated side.

C. Power supply

A medical grade power supply (SRP-100-4002, TRC Electronics, Inc.) which meets EN 60601-1 is used to power all of the circuitry. Although all of the electronic components are isolated, the computer is also an integral part of the system, and therefore it also requires isolation, so the entire system is fed via another isolation transformer.

V. SOFTWARE

A. Generating an image

LABVIEW™ is used as the control software. The software displays two images of [Hb] and [HbO₂] in a pixel format (a single image consists of 56 pixels,) and a graph of [Hb] and

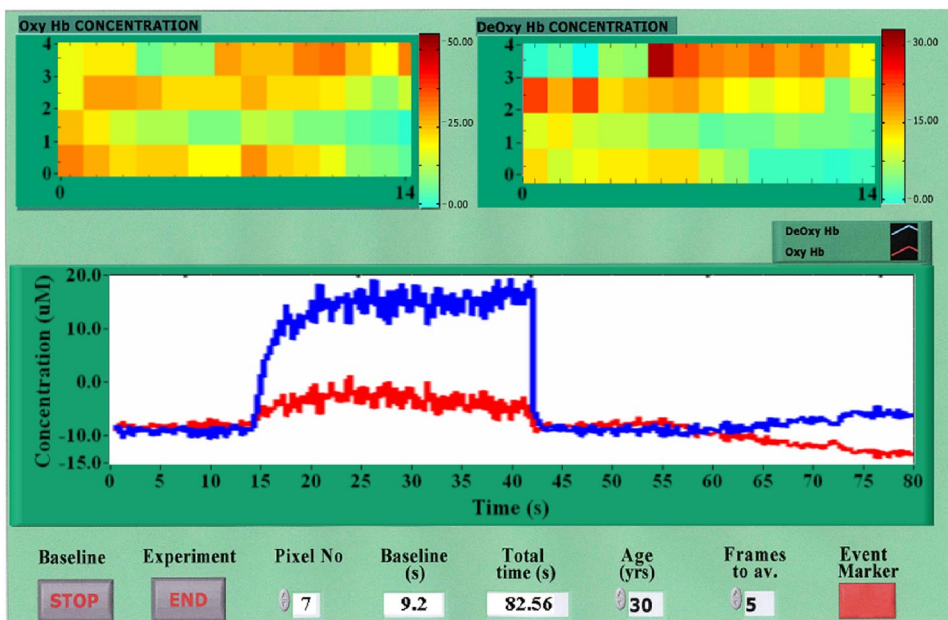


FIG. 4. (Color online) LABVIEW™ user interface. The front panel shows the instantaneous value of (Hb) and (HbO_2) on all 56 pixels (top). The user can view an individual pixel by selecting the appropriate “Pixel No.” and a trace will be displayed (pixel 7 is on display on the bottom trace).

[HbO_2] in real time at a rate of 3 Hz (Fig. 4). The sequence of activating the LEDs and monitoring the photodiode output is all under software control. The hardware has been designed for multiple LEDs to be illuminated, provided that there is negligible cross talk from the detected signals. Currently, a simple pulsing scheme is employed, where only one LED is illuminated at a time. The 780-nm LED is pulsed, then the 880-nm LED at location A with the detected signal by PD 1 assigned to pixel 1 (Fig. 2). This process is repeated for locations B to X. This simple pulsing scheme produces a frame rate of 3 Hz. However, a faster acquisition of 20 Hz can be obtained if multiple LEDs are illuminated. For example, LEDs A, E, Q, and T could simultaneously be turned on and the corresponding voltages produced at nearest photodiodes measured. Since the LEDs that are turned “on” are far apart, there will be negligible cross talk and interference in the detected signals at the photodiodes. However, this faster acquisition scheme has not been implemented, but will be in the near future.

The user interface requires the user to press only three buttons: one to start acquiring a baseline signal, one to stop acquisition of baseline, and another to indicate the end of the data acquisition (Fig. 4). There are three stages involved in data acquisition: measurement of dark current, measurement of baseline, and acquisition during stimulus. Initially, the dark current signal from each photodiode is measured with all of the LEDs turned off. This current is subtracted from all subsequent readings; the baseline signal is obtained as the LEDs are pulsed sequentially for a user-specified time. The measured intensities for each pixel are stored in an array following acquisition of the entire set of baseline data, and an average for each pixel for the entire period is calculated. This average value is automatically subtracted from the pixel value measured during the stimulus period.

To convert changes in intensities into changes in chromophore concentration, it is necessary to make the assumption that there are only two wavelength-dependent chromophores (Hb and HbO_2) in the tissue being interrogated.

The extinction coefficients for these two chromophores are well known,³³ but since the LEDs emit light over a relatively broad wavelength range, the extinction coefficient for the two chromophores cannot be taken as a single value at the nominal center wavelengths of 780 and 880 nm. The spectrum has to be normalized and weighted according to the extinction coefficient and emitted intensities at each wavelength. To ensure accuracy, the spectra of all 48 LEDs were measured with a spectrometer. For the 780-nm LEDs, the mean peak wavelength was found to be 787.8 nm (range 771.1–794.0 nm). For the 880-nm LED, the mean peak wavelength was 878.8 nm (range 880.8–875.1 nm).

VI. EXPERIMENTAL STUDIES

A. Experiments on phantom: Sensitivity of the system

Studies on tissue equivalent phantoms were conducted to test the spatial sensitivity of the system, and in particular the depth at which signals can be obtained. The flexible pad was placed beneath a rectangular tank ($60 \times 90 \times 70$ mm), which had a thin base (2 mm) made of a tissue-equivalent epoxy resin.³⁴ The tank itself was filled with an Intralipid solution with optical properties similar to those of the neonatal brain ($\mu_a = 0.008 \text{ mm}^{-1}$ and $\mu'_s = 0.9 \text{ mm}^{-1}$) and a black rod (diameter 10 mm, length 90 mm) attached to an xyz translation stage was positioned vertically in the tank.³⁵ The 880-nm LED at location L (Fig. 2) was illuminated and the output voltage from two photodiodes (PD3 and PD2) at two different separations from the source (11 and 27 mm) was monitored continuously as the black rod was raster scanned in steps of 2 mm in the x , y , and z directions. Figure 5(a) shows the area scanned, including the LEDs and photodiodes that were monitored.

To test how well the experimental results compared with theoretical prediction, a finite element-based model of photon diffusion in tissues (TOAST), which was developed at University College London (UCL),³⁶ was used to model the

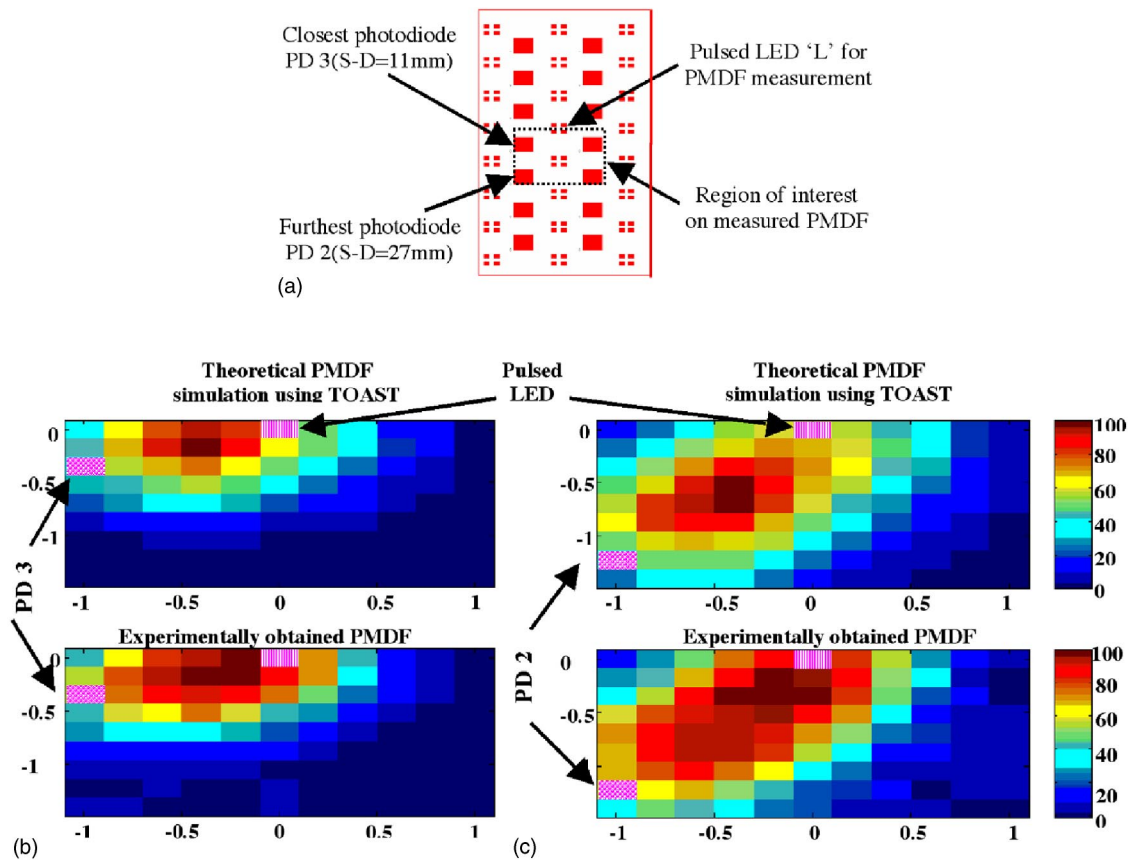


FIG. 5. (Color online) Software simulation on TOAST. (a) Diagram showing the source detector arrangement for depth and PMDF simulation/measurement. The comparison of theoretically simulated and experimentally measured PMDFs for source to detector separations of (b) 11 and (c) 27 mm.

experimental setup.^{37,38} The rectangular tank (60×90×70 mm) was modeled, including correct information about the size of the detector and source, together with necessary boundary conditions (Robin/Type III). The calculated photon measuring density functions (PMDF)³⁹ for the two source and detector separations (11 and 27 mm) are also shown in Figs. 5(b) and 5(c), and show good agreement with the experimentally measured data.

In order to estimate the maximum penetration depth of the signal, a black rod was placed at the point of maximum sensitivity (100%) for each source detector separation, and the detected signal was recorded as the rod was raised vertically in steps of 1 mm. Figure 6 shows the resulting signals plotted versus depth. The maximum penetration depth was defined as the point where the change in signal is equal to the system noise. For source detector separations of 11 and

27 mm, the experimentally measured maximum depths that can be probed are 6 and 12 mm, respectively. This depth of penetration is suitable for measurements on babies and the NIR light will be able to penetrate the relatively thin overlying layers of skin and skull.

B. Temperature rise

The power dissipated by the 14 photodiode amplifiers mounted on the flexible pad will cause the temperature of the pad to increase, since the silicone encapsulant has a high thermal resistance (90 °C/W). It was necessary to confirm whether this temperature rise remained below the maximum permissible skin temperature. Temperature rise was therefore monitored using a thermocouple (K type) placed between the pad and the forehead of a volunteer. Measurements were performed for 1 h with the thermocouple placed at two loca-

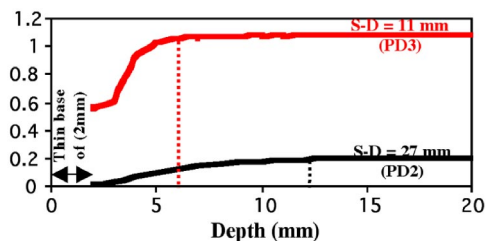


FIG. 6. (Color online) Depth sensitivity profile for two source-detector separations measured at the point of maximum sensitivity. The dotted lines represent the depths at which the signal change equals the residual system noise.

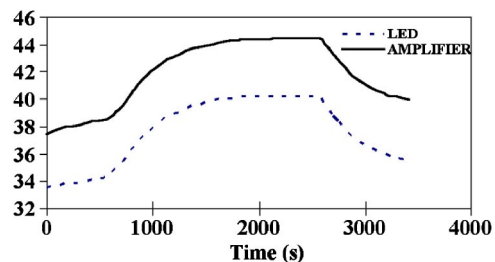


FIG. 7. (Color online) The temperature rise on the skin beneath the flexible pad measured directly under the amplifier and the LED.

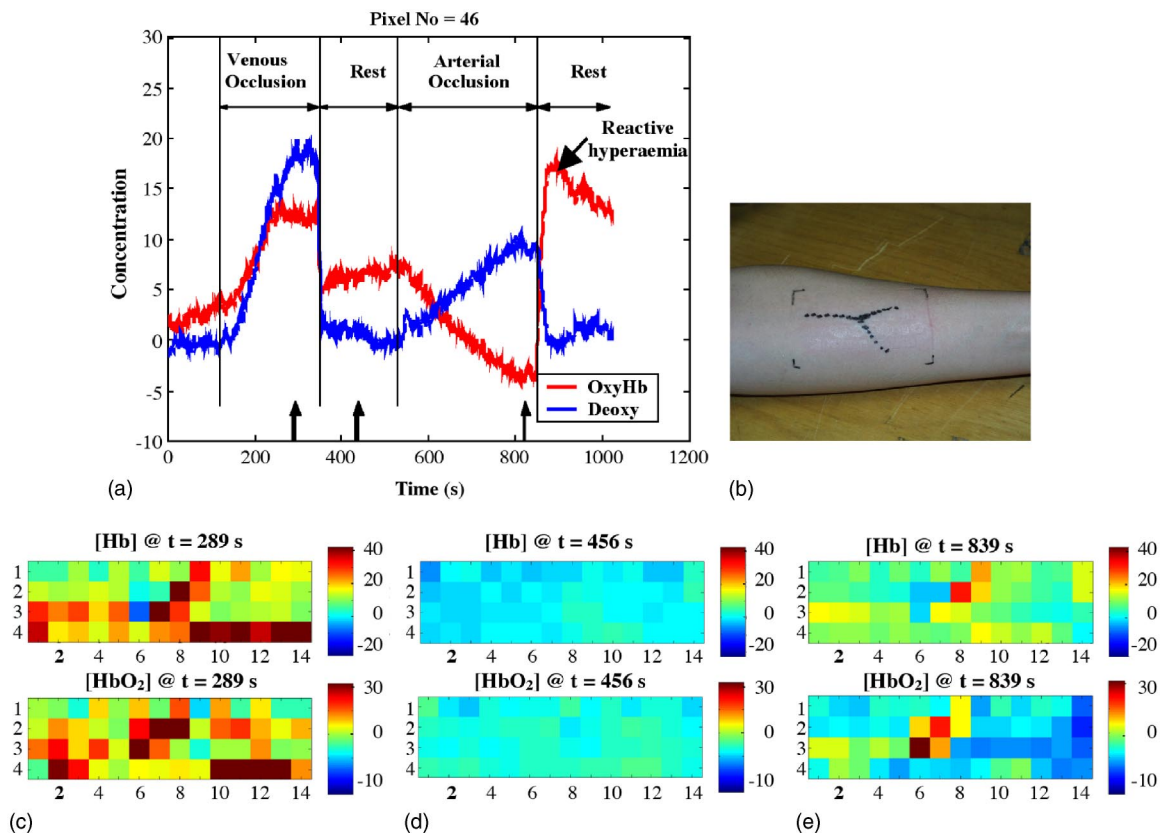


FIG. 8. (Color online) Pressure cuff occlusion experiments. (a) A typical [Hb] and [HbO₂] plot obtained at one pixel during the experiment. (b) A picture outlining the veins seen on the surface and the corresponding [Hb] and [HbO₂] maps obtained during (c) venous occlusion, (d) rest, and (e) arterial occlusion.

tions: one was directly under a photodiode/amplifier and the other under an LED (Fig. 7). The maximum observed temperature of 40 °C, which only occurred after 30 min, is within the normally allowed temperature for skin exposure periods of <4 h.

C. Pressure cuff measurements

There are currently no validated neonatal cerebral evoked response tests against which this instrument can be calibrated. In order to demonstrate the system performance on a physiological signal, we therefore carried out measurements on the forearm of adult volunteers, looking at the changes that occur in response to venous and arterial occlusion as has previously been demonstrated.^{9,40,41} Six male and six female normal healthy volunteers had the flexible pad attached to the underside of the lower forearm and a blood pressure cuff was placed around their upper arm. The data acquisition protocol was as follows: (a) 0–120 s baseline recording; (b) 120–360 s venous cuff occlusion at 40 mm Hg; (c) 360 s venous cuff release; (d) 360–540 s rest; (e) 540–920 s arterial cuff occlusion at 200 mm Hg; and (f) 920 s cuff release and recovery. Figure 8(a) is a typical plot of the Hb and HbO₂ changes measured from one pixel (46) during this procedure, while Fig. 8(c) shows images of Hb and HbO₂ changes obtained at the three time points indicated in Fig. 1.

The results seen in Fig. 8(a) match well the changes one would expect in both [Hb] and [HbO₂] during these maneuvers. During venous occlusion, both [Hb] and [HbO₂] should

rise as the normal venous return is restricted while arterial blood continues to flow into the arm, resulting in blood pooling. During arterial occlusion, all blood flow into the arm ceases (ignoring bone blood flow), but the tissue continues to consume oxygen, resulting in a decrease in [HbO₂] and a matching increase in [Hb]. Upon release of the arterial occlusion, reactive hyperaemia is also visible (due to the sudden inrush of arterial blood). The images in Figs. 8(c)–8(e) show the distribution of [Hb] and [HbO₂] changes in the arm, and the time course of these changes can be seen as a movie, accessible on www.medphys.ucl.ac.uk/~tharshan/forearm.html. What is noticed in the images taken during venous occlusion is a horizontal, branching feature of the pixels with noticeably higher hemoglobin concentrations. These are due to the presence of larger surface veins just below the skin surface on the arm, and Fig. 8(b) shows the arm with the corresponding surface veins marked with black ink. Preliminary studies have already been conducted on babies who were given a checkerboard visual stimulus, where the system showed both good temporal and spatial resolution.³⁷

ACKNOWLEDGMENTS

This research was generously funded by Action Research and Hamamatsu Photonics K.K.

¹F. F. Jöbsis, *Science* **198**, 1264 (1977).

²T. Kato, A. Kamei, S. Takashima, and T. Ozaki, *J. Cereb. Blood Flow Metab.* **13**, 516 (1993).

- ³J. H. Meek, M. Firbank, C. E. Elwell, J. Atkinson, O. Braddick, and J. S. Wyatt, *Pediatr. Res.* **43**, 840 (1998).
- ⁴J. S. Wyatt, M. Cope, D. T. Delpy, A. D. Edwards, S. C. Wray, and E. O. R. Reynolds, *Lancet* **2**, 1063 (1986).
- ⁵A. Villringer, J. Planck, C. Hock, L. Schleinkofer, and U. Dirnagle, *Neurosci. Lett.* **154**, 101 (1993).
- ⁶F. E. W. Schmidt, M. E. Fry, E. M. C. Hillman, J. C. Hebden, and D. T. Delpy, *Rev. Sci. Instrum.* **71**, 256 (2002).
- ⁷B. Chance, J. Glickson, R. Weissleder, C. Tung, D. Blessington, and S. Zhou, *OSA Proc. Adv. Opt. Imaging Photon Migration 450* (2002).
- ⁸J. Hulvershorn, L. Bloy, J. S. Leigh, and M. A. Elliot, *Rev. Sci. Instrum.* **74**, 4150 (2003).
- ⁹N. B. Hampson and C. A. Piantadosi, *J. Appl. Physiol.* **64**, 2449 (1988).
- ¹⁰V. Ntziachristos, X. Ma, and B. Chance, *Rev. Sci. Instrum.* **69**, 4221 (1998).
- ¹¹V. Ntziachristos, X. H. Ma, A. G. Yodh, and B. Chance, *Rev. Sci. Instrum.* **70**, 193 (1999).
- ¹²D. Grosenick, H. Wabnitz, H. H. Rinneberg, K. T. Moesta, and P. M. Schlag, *Appl. Opt.* **38**, 2927 (1999).
- ¹³H. Eda, I. Oda, Y. Ito, Y. Wada, Y. Oikawa, Y. Tsunazawa, M. Takada, Y. Tsuchiya, Y. Yamashita, M. Oda, A. Sassaroli, Y. Yamada, and M. Tamura, *Rev. Sci. Instrum.* **70**, 3595 (1999).
- ¹⁴M. A. O'Leary, D. A. Boas, and B. Chance, *Opt. Lett.* **20**, 426 (1995).
- ¹⁵G. Taga, Y. Konishi, A. Maki, T. Tachibana, M. Fujiwara, and H. Koizumi, *Neurosci. Lett.* **282**, 101 (2000).
- ¹⁶M. Pena, A. Maki, and D. Kovacic, *Proc. Natl. Acad. Sci. U.S.A.* **100**, 11702 (2003).
- ¹⁷G. Taga, K. Asakawa, and A. Maki, *Proc. Natl. Acad. Sci. U.S.A.* **100**, 10722 (2003).
- ¹⁸A. Maki, Y. Yamashita, Y. Ito, E. Watanabe, Y. Mayanagi, and H. Koizumi, *Med. Phys.* **22**, 1997 (1995).
- ¹⁹N. Ramanujam, C. Du, H. Y. Ma, and B. Chance, *Rev. Sci. Instrum.* **69**, 3042 (1998).
- ²⁰T. O. McBride, B. W. Pogue, S. Jiang, Österberg, and K. D. Paulsen, *Rev. Sci. Instrum.* **72**, 1817 (2001).
- ²¹B. Chance, K. A. Kang, L. He, H. Liu, and S. Zhou, *Rev. Sci. Instrum.* **67**, 4324 (1996).
- ²²T. Pham, O. Coquoz, J. B. Fishkin, E. Anderson, and B. J. Tromberg, *Rev. Sci. Instrum.* **71**, 2500 (2000).
- ²³C. H. Schmitz, M. Locker, J. M. Lasker, A. H. Hielscher, and R. L. Barbour, *Rev. Sci. Instrum.* **73**, 429 (2002).
- ²⁴M. Niwayama, D. Kohata, J. Shao, N. Kudo, T. Hamaoka, T. Katsumura, and K. Yamamoto, *Proc. SPIE* **4082**, 48 (2000).
- ²⁵Y. Lin, S. Lech, X. Nioka, X. Intes, and B. Chance, *Rev. Sci. Instrum.* **73**, 3065 (2002).
- ²⁶A. M. Siegel, J. J. A. Marota, and D. A. Boas, *Opt. Express* **4**, 287 (1999).
- ²⁷V. Ntziachristos, H. Ma, A. G. Yodh, and B. Chance, *Rev. Sci. Instrum.* **70**, 193 (1999).
- ²⁸S. Hintz, D. A. Benaron, A. Siegel, A. Zourabain, D. K. Stevenson, and D. A. Boas, *J. Perinat. Med.* **29**, 335 (2001).
- ²⁹M. Franceschini, V. Toronov, M. Filiaci, E. Gratton, and S. Fantini, *Opt. Express* **6**, 49 (2000).
- ³⁰G. Taga, K. Asakawa, A. Maki, Y. Konishi, and H. Koizumi, Presented at the 8th International Conference on Functional Mapping of the Human Brain, 2–6 June 2002, Sendai, Japan (available on CD-Rom in *Neuroimage*, Vol. 16, No. 2).
- ³¹Y. Yamashita, A. Maki, and H. Koizumi, *Med. Phys.* **28**, 1108 (2001).
- ³²J. G. Graeme, *Photodiode Amplifiers: Op Amp Solutions* (McGraw-Hill, New York, 1996).
- ³³S. Matcher, C. E. Elwell, M. Cope, and D. T. Delpy, *Anal. Biochem.* **227**, 54 (1995).
- ³⁴M. Firbank and D. T. Delpy, *Phys. Med. Biol.* **38**, 847 (1993).
- ³⁵T. Vaithianathan, I. Tullis, N. Everdell, T. Leung, J. Meek, and D. T. Delpy, *Proc. SPIE* **4955**, 96 (2003).
- ³⁶M. Schweiger, S. R. Arridge, and D. T. Delpy, *J. Math. Imaging Vision* **3**, 263 (1993).
- ³⁷S. R. Arridge and J. C. Hebden, *Phys. Med. Biol.* **42**, 841 (1997).
- ³⁸S. R. Arridge, *Inverse Probl. Eng.* **15**, R41 (1999).
- ³⁹S. R. Arridge and M. Schweiger, *Appl. Opt.* **34**, 8026 (1995).
- ⁴⁰B. Chance, E. Borer, A. Evans, G. Holtom, J. Kent, M. Maris, K. McCully, J. Northrop, and M. Shinkwin, *Ann. N.Y. Acad. Sci.* **551**, 1 (1988).
- ⁴¹B. Chance, S. Nioka, J. Kent, K. McCully, M. Fountain, R. Greenfield, and G. Holtom, *Anal. Biochem.* **174**, 698 (1988).